Mon. Not. R. Astron. Soc. **343,** 552–558 (2003)

Concerning the connection between the C_ℓ power spectrum of the cosmic microwave background and the Γ_m Fourier spectrum of rings on the sky

R. Ansari,[1] S. Bargot,[1] A. Bourrachot,[1] F. Couchot,[1] J. Haïssinski,[1] S. Henrot-Versillé,[1] G. Le Meur,[1] O. Perdereau,[1⋆] M. Piat,[2] S. Plaszczynski[1] and F. Touze[1]

[1] *Laboratoire de l'Accélérateur Linéaire, IN2P3-CNRS and Université de Paris-Sud, BP 34, 91898 Orsay Cedex, France*
[2] *Institut d'Astrophysique Spatiale, INSU-CNRS and Université de Paris-Sud, 91405 Orsay Cedex, France*

Accepted 2003 April 7. Received 2003 January 28

ABSTRACT

In this article we present and study a scaling law of the $m\Gamma_m$ cosmic microwave background Fourier spectrum on rings that allows us to (i) combine spectra corresponding to different colatitude angles (e.g. several detectors at the focal plane of a telescope) and (ii) recover the C_ℓ power spectrum once the Γ_m coefficients have been measured. This recovery is performed numerically below the 1 per cent level for colatitudes $\Theta > 80^\circ$. In addition, taking advantage of the smoothness of C_ℓ and of Γ_m, we provide analytical expressions that allow the recovery of one of the spectra at the 1 per cent level, the other one being known.

Key words: cosmic microwave background.

1 FOURIER ANALYSIS OF CIRCLES ON THE SKY VERSUS SPHERICAL HARMONICS EXPANSION

Cosmic microwave background (CMB) exploration has recently made great progress thanks to balloon-borne experiments (BOOMERANG, Mauskopf et al. 2000; MAXIMA, Hanany et al. 2000; Archeops, Benoît et al. 2003) and ground-based interferometers (CBI, Contaldi et al. 2002; DASI, Halverson et al. 2002; VSA, Taylor et al. 2003). *MAP*,[1] the first results from which will be available at the beginning of 2003, and the forthcoming *Planck* satellite,[2] the launch of which is scheduled for the beginning of 2007 will scan the entire sky with resolutions of 20 and 5 arcmin, respectively. These CMB observation programmes yield a large amount of data, the reduction of which is usually performed through a map-making process and then by expanding the temperature inhomogeneities on the spherical harmonics basis:

$$\frac{\Delta T(\boldsymbol{n})}{T} = \sum_{\ell} \sum_{m=-\ell}^{\ell} a_{\ell m} Y_{\ell m}(\boldsymbol{n}). \tag{1}$$

The outcome of the measurements is given in the form of the angular power spectrum $C_\ell \equiv \langle |a_{\ell m}|^2 \rangle$. The set of C_ℓ coefficients completely characterizes the CMB anisotropies in the case of uncorrelated Gaussian inhomogeneities (Bond & Efstathiou 1987; Hu & Dodelson 2002).

Several of the current or planned CMB experiments (Archeops, *MAP*, *Planck*) perform or will perform circular scans on the sky. Carrying out a one-dimensional analysis of the CMB inhomogeneities on rings provides a valuable alternative to characterize its statistical properties (Delabrouille et al. 1998). A ring-based analysis looks promising, for example, for the *Planck* experiment where repeated (∼60 times) scans of large circles with a colatitude angle $\Theta \sim 85^\circ$ are being planned. This approach differs in several ways from that based on spherical harmonics. In particular, it does not require the construction of sky maps and some systematic effects could be easier to treat in the time domain rather than in two-dimensional (Θ, φ) space ($1/f$ noise for instance), since the map-making procedure involves a complex projection on to this space.

For a circle of colatitude Θ, one writes

$$\frac{\Delta T(\Theta, \varphi)}{T} = \sum_{m=-\infty}^{+\infty} \alpha_m(\Theta) \mathrm{e}^{\mathrm{i}m\varphi} \tag{2}$$

and the Γ_m Fourier spectrum is defined by

$$\left\langle \alpha_m \alpha^*_{m'} \right\rangle = \Gamma_m(\Theta) \delta_{mm'}. \tag{3}$$

These Γ_m coefficients are thus specific to a particular colatitude angle Θ. Below, we propose a simple way of combining sets of such coefficients corresponding to different Θ values (i.e. different detectors).

Fig. 1 shows an example of the C_ℓ power spectrum for $\ell < 1500$, together with two Fourier spectra,[3] which describe the same sky for two quite distinct cases, one for $\Theta = 90^\circ$ and one for $\Theta = 40^\circ$.

Note that for this figure and throughout the article the C_0 and C_1 coefficients have been set equal to 0.

⋆E-mail: perderos@lal.in2p3.fr

[1] *MAP* home page: http://map.gsfc.nasa.gov/

[2] *Planck* home page: http://astro.estec.esa.nl/SA-general/Projects/Planck/

[3] Note that we have chosen the following normalizations: the C_ℓ coefficients have been multiplied by $\ell(2\ell + 1)/4\pi$ and Γ_m by $2m$.

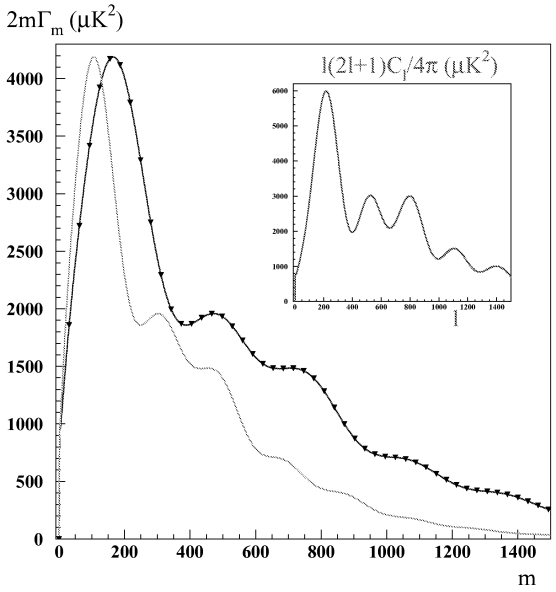

Figure 1. 'Typical' power spectra. The inset shows a $\ell(2\ell+1)C_\ell/4\pi$ spectrum up to $\ell = 1500$. The main graphs are two Fourier spectra ($2m\Gamma_m$) calculated exactly using equation (4): one for $\Theta = 90°$ (darker curve) and the other for $\Theta = 40°$ (lighter curve). The triangles represent a subsample of the $2m\Gamma_m(\Theta = 40°)$ coefficients after having rescaled their abscissa by a factor $1/\sin 40° = 1.556$.

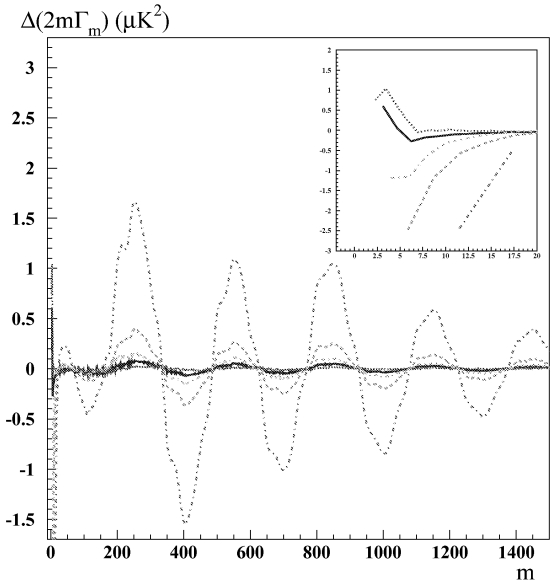

Figure 2. Absolute differences (in μK^2) between $2m\Gamma_m(\Theta)$ spectra scaled to $\Theta = 90°$ and the interpolated $2m\Gamma_m(\Theta = 90°)$ spectrum. All spectra are based on the C_ℓ spectrum of Fig. 1. We have worked out these differences for $\Theta = 60°$ (smallest amplitude curve), 40°, 30°, 20° and 10° (largest amplitude curve). The inset displays the low-m part, showing that the difference has a meaningful value only above $m = 2/\sin\Theta$.

The relation that gives $\Gamma_m(\Theta)$ from C_ℓ was obtained by Delabrouille et al. (1998):

$$\Gamma_m(\Theta) = \sum_{\ell=|m|}^{\infty} C_\ell B_\ell^2 \mathcal{P}_{\ell m}^2(\cos\Theta), \tag{4}$$

where the set of B_ℓ coefficients characterizes the beam function and $\mathcal{P}_{\ell m}^2$ are the normalized associated Legendre functions. This relation assumes that $a_{\ell m}$ introduced in equation (1) are uncorrelated Gaussian random variables and that the scan is performed with a symmetric beam.

In this article, we present the scaling law and the inverse transformation that consists in the calculation of C_ℓ from Γ_m. In Section 2, we demonstrate that this simple scaling law, displayed by the $m\Gamma_m$ spectrum for different colatitude angles, is accurate. Section 3 is dedicated to the description of two different methods proposed to invert equation (4) in the case where $\Theta = 90°$. While a simple matrix inversion leads to the result, we also present an approximate analytic method. In Section 4 these two methods are extended to the general case where $\Theta < 90°$.

2 SCALING OF THE $m\Gamma_m(\Theta)$ SPECTRUM

Our study was triggered by one of us noticing that the product $m\Gamma_m(\Theta)$ is only a function of the reduced variable $\mu \equiv m/\sin\Theta$, i.e. this product is independent (to a very good approximation) of the colatitude angle Θ.

This scaling is illustrated in Fig. 1, where a $2m\Gamma_m$ spectrum computed for a colatitude angle of $\Theta = 40°$ is scaled to match the corresponding $\Theta = 90°$ one. To quantify the precision of this approximate scaling law, we have computed the differences between the scaled $2m\Gamma_m(\Theta)$ and the interpolated $2m\Gamma_m(\Theta = 90°)$ spectrum (at $m/\sin\Theta$). Examples are shown in Fig. 2 for five Θ values ranging between 60° and 10°. The absolute values of these differences are lower than 2 μK^2 over the whole m range for the particular spectrum given in Fig. 1. They are only defined for m values greater than $2/\sin\Theta$, as shown in the inset. Oscillations are observed in the difference. They present the same period but their amplitudes increase as the colatitude angle Θ decreases.

Different $2m\Gamma_m(\Theta)$ sets obtained from several detectors over a small range of colatitude angles Θ (a few degrees) may be combined using this scaling law, with a precision better than 0.01 per cent. Several experiments, spanning a wider range of colatitude angles, may also be combined likewise, however, with a slightly worse precision.

In the following, we explain this scaling law using a geometrical and a mathematical argument.

2.1 Geometric interpretation

The power spectrum $\Gamma_m(\Theta)$ is the Fourier transform of the signal autocorrelation function $A(\delta\phi, \Theta)$, where $\delta\phi$ is the phase difference between two points of the scanned ring. Two such points have an angular separation $\delta\psi$ on the unit sphere, where

$$\delta\psi = 2\arcsin\left(\sin\Theta\sin\frac{\delta\phi}{2}\right). \tag{5}$$

This relation between $\delta\phi$ and $\delta\psi$ allows one to express the scaling law, since the signal autocorrelation function, expressed as a function of $\delta\psi$ is equal to the autocorrelation function on a large-circle scan:

$$A(\delta\psi, \pi/2) = A(\delta\phi, \Theta). \tag{6}$$

For small $\delta\phi$, this relation becomes linear:

$$\delta\psi = \sin\Theta\,\delta\phi. \tag{7}$$

So that, in this linear regime, the autocorrelation function satisfies

$$A(\delta\phi, \Theta) = A(\sin\Theta\delta\phi, \pi/2). \tag{8}$$

Since the ring length L on the unit sphere is $2\pi\sin\Theta$, the mth harmonic of the Fourier expansion corresponds to structures on the sky of angular size

$$\lambda \equiv 2\pi\frac{\sin\Theta}{m} = \frac{2\pi}{\mu}. \tag{9}$$

In the continuum approximation, taking the Fourier transform of both sides of equation (8) leads to

$$\Gamma_m(\Theta) = \frac{1}{\sin\Theta}\Gamma_{m/\sin\Theta}(\pi/2), \tag{10}$$

which, using equation (9) leads to the scaling law

$$m\Gamma_m(\Theta) = \mu\Gamma_\mu(\pi/2). \tag{11}$$

While we are mainly concerned here with circular scanning, the same reasoning can be made for any kind of trajectory on the sky as long as it stays 'close' to a large circle on angular scales of the order of λ, and the same scaling law applies to the power density spectrum expressed as a function of $1/\lambda$.

2.2 Analytic interpretation

To investigate this scaling mathematically, we start from equation (4), which gives the exact relations that connect $\Gamma_m(\Theta)$ to C_ℓ. Since B_ℓ are, supposedly, well-known quantities for each experimental set-up, we will no longer mention them explicitly and we will deal with the coefficients $\mathcal{C}_\ell \equiv C_\ell B_\ell^2$.

We calculate the $\mathcal{P}^2_{\ell m}(\cos\Theta)$ factors using approximate expressions of the Legendre associated functions given by Robin (1957) (see Appendix A for some details) which, once normalized, read as follows.

(i) For $\ell < m/\sin\Theta$,

$$\mathcal{P}_{\ell m}(\cos\Theta) \simeq \frac{1}{2\pi}\sqrt{\frac{\ell+1/2}{M}}\left(\frac{\ell\cos\Theta + M}{\ell}\right)^{\ell+1/2} \times \left[\frac{m\cos\Theta - M}{(\ell-m)\sin\Theta}\right]^m \prod_{k=1}^{m}\sqrt{\frac{\ell+k-m}{\ell+k}}, \tag{12a}$$

where $M = \sqrt{m^2 - \ell^2\sin^2\Theta}$,

(ii) and for $\ell > m/\sin\Theta$,

$$\mathcal{P}_{\ell m}(\cos\Theta) \simeq \frac{(-1)^m}{2\pi}\sqrt{\frac{2(2\ell+1)}{N}}\cos\omega, \tag{12b}$$

where $N = \sqrt{l^2\sin^2\Theta - m^2}$. The expression for the angle ω is given in Appendix A. These approximations are illustrated in Fig. 3.

For $\ell < m/\sin\Theta$, the numerical value of $\mathcal{P}^2_{\ell m}(\cos\Theta)$ is negligible, while for $\ell > m/\sin\Theta$ equation (12b) implies

$$\mathcal{P}^2_{\ell m}(\cos\Theta) \simeq \frac{1}{4\pi^2}\frac{2\ell+1}{(\ell^2\sin^2\Theta - m^2)^{1/2}}[1+\cos(2\omega)]. \tag{13}$$

Since the CMB angular power spectrum varies slowly as a function of ℓ, we may replace the sum over ℓ in equation (4) by an integral. We thus obtain

$$m\Gamma_m(\Theta) = \frac{m}{4\pi^2}\int_{m/\sin\Theta}^{\ell_{\max}}\frac{\mathcal{C}(\ell)[2\ell+1][1+\cos(2\omega)]}{(\ell^2\sin^2\Theta - m^2)^{1/2}}\,\mathrm{d}\ell \tag{14}$$

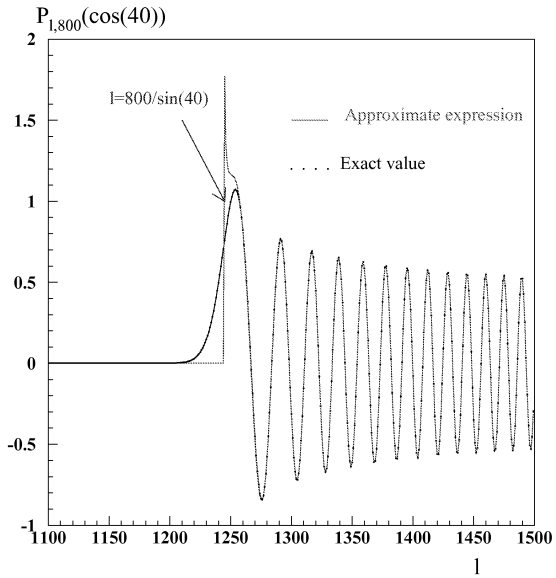

Figure 3. Comparison between the exact value of $\mathcal{P}_{\ell 800}(\cos 40^\circ)$ as a function of ℓ (dotted line) and that obtained with the approximate expressions of equations (12a) and (12b) (solid line). The arrow indicates the $\ell = 800/\sin 40^\circ$ abscissa.

where $\ell_{\max}$ is an ℓ value beyond which the power spectrum vanishes, and $\mathcal{C}(\ell)$ is a function of $\ell \in [0, \ell_{\max}]$ that smoothly interpolates the $\mathcal{C}_\ell$ coefficients (a simple way of proceeding is given in Appendix B).

The oscillation frequency ν of the cosine term (as a function of ℓ) in the integrand in the right-hand side of equation (14) is of the order of Θ/π (thus $\nu \sim 1/2$ when $\Theta = \pi/2$). Such a frequency is high enough for this cosine term to contribute only a very small amount to the integral. This will be checked numerically in Section 3.1 below. Thus, we may write

$$m\Gamma_m(\Theta) \simeq \frac{1}{4\pi^2}\int_{\mu}^{\ell_{\max}}\mathcal{C}(\ell)\frac{2\ell+1}{[(\ell/\mu)^2-1]^{1/2}}\,\mathrm{d}\ell. \tag{15}$$

This equation demonstrates – within the approximations that have been made – that the product $m\Gamma_m(\Theta)$ depends only on the variable $\mu = m/\sin\Theta$.

Since the variable μ is not constrained to be an integer, one has to introduce a smooth function, $\Gamma(m, \Theta)$, where m is now a real, that interpolates the $\Gamma_m(\Theta)$ discrete spectrum. This can be done in the same way as that indicated for the $\mathcal{C}_\ell$ spectrum (cf. Appendix B).

In terms of this $\Gamma(m, \Theta)$ function, the scaling law is expressed by the relation

$$\Gamma(m', \Theta') = \frac{\sin\Theta}{\sin\Theta'}\Gamma\left(m'\frac{\sin\Theta}{\sin\Theta'}, \Theta\right). \tag{16}$$

This equation follows from the equality $m\,\Gamma(m, \Theta) = m'\Gamma(m', \Theta')$, which holds true provided that $m/\sin\Theta = m'/\sin\Theta'$.

Assuming that the Fourier spectrum has been obtained for a particular value Θ of the colatitude angle, equation (16) allows one to calculate $\Gamma(m', \Theta')$ for $m' = m\sin\Theta'/\sin\Theta$, $m = 1, 2, \ldots, m_{\max} = \ell_{\max}\sin\Theta$. Then, by interpolation, one obtains $\Gamma(m', \Theta')$ for all integer values of m' ranging from $\sin\Theta'/\sin\Theta$ up to $\ell_{\max}\sin\Theta'$. Equation (16) can thus be used to compare and combine Fourier spectra that correspond to different Θ values.

3 RECOVERING THE $\mathcal{C}_\ell$ COEFFICIENTS FROM THE $\Gamma_m(\pi/2)$ FOURIER SPECTRUM

3.1 Checking and solving the integral equation that relates $\mathcal{C}(\ell)$ to $\Gamma\,(m, \pi/2)$

Since Θ is assumed to be equal to $\pi/2$ in this section, the variable μ can be identified with m.

In order to facilitate the numerical calculation of the right-hand side of equation (15), we introduce a new variable of integration x defined by $\ell = m\cosh x$. Then equation (15) can be rewritten as

$$\Gamma(m, \pi/2) = \frac{1}{4\pi^2} \times \int_0^{\cosh^{-1}(\ell_{\max}/m)} (2m\cosh x + 1)\mathcal{C}(m\cosh x)\,\mathrm{d}x. \tag{17}$$

The transformation defined by equation (17) is linear: thus one may insert in the integrand an interpolating function of the $\mathcal{C}_\ell$ spectrum as defined by equation (B1). The output of equation (17) applied to the angular power spectrum of Fig. 1 is shown in Fig. 4. One can see in this figure that for such a spectrum the approximations made in Section 2 ensure an accuracy of better than 1 per cent – except at the lower end of the spectrum where the relative error drops below 2 per cent for $m = 14$.

Equation (17) can be solved for $\mathcal{C}(\ell)$ by noticing that this integral equation is similar to Schlömilch's equation, which reads

$$F(m) = \frac{2}{\pi}\int_0^{\pi/2} \Phi(m\sin x)\,\mathrm{d}x, \tag{18}$$

where m is real.

The way to solve the latter equation can be found, for example, in Kraznov et al. (1977). We proceed in a similar way for equation (17) (the details are given in Appendix C) and we obtain

$$\mathcal{C}(\ell) = -8\pi\frac{\ell}{2\ell+1}\int_0^{\cosh^{-1}(\ell_{\max}/\ell)} \Gamma'(\ell\cosh x)\,\mathrm{d}x, \tag{19}$$

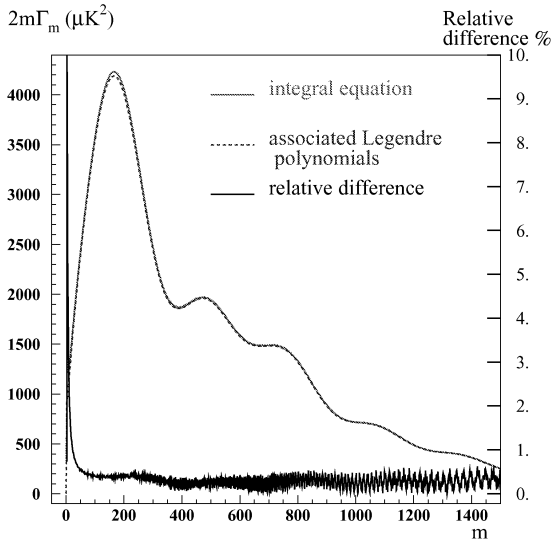

Figure 4. Comparison between the $2m\Gamma_m$ coefficients computed with the associated Legendre polynomials (dashed line) and the $2m\Gamma(m)$ function calculated using equations (17), (B1) and (B2) with $\sigma = 0.5$ (solid line). The relative difference between the results of the two calculations is shown by the lower curve (in per cent, right-hand scale).

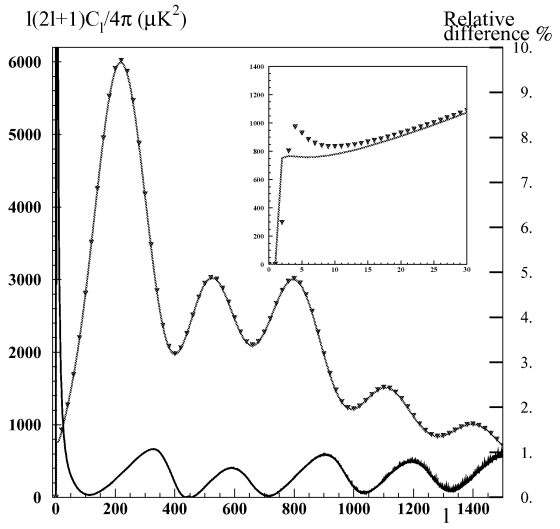

Figure 5. Comparison between the 'typical' $\mathcal{C}_\ell$ coefficients for $\Theta = 90°$ (solid line), used to calculate the Γ_m Fourier spectrum [using the $\mathbf{P}(\mathbf{0})$ matrix] and the $\mathcal{C}(\ell)$ function obtained by inserting this Fourier spectrum in equation (19), (triangles; only some points are shown). We have set $\sigma = 1$ in equation (B2). The relative difference (in per cent) is shown by the lower curve (right-hand scale). Inset: close-up of the low-ℓ region.

where Γ' is the derivative of $\Gamma\,(m, \pi/2)$ with respect to m. Again the transformation implied by equation (19) is a linear one, allowing the use of interpolating functions as defined in Appendix B. Fig. 5 illustrates the use of this integral equation to calculate the $\mathcal{C}_\ell$ coefficients starting with the set of $\Gamma_m(\pi/2)$ values.

3.2 Numerical inversion

In the $\Theta = \pi/2$ case, the connection between the set of C_ℓ values and the corresponding Γ_m values is simple since equation (4) can be written using matrices (Piat et al. 2002):

$$\boldsymbol{\Gamma} = \mathbf{P}(\mathbf{0}) \times \boldsymbol{\mathcal{C}}, \tag{20}$$

with

$$\mathbf{P}(\mathbf{0})_{ij} = [\mathcal{P}_{ji}(0)]^2, \tag{21}$$

where $\mathcal{P}_{ji}$ are the normalized associated Legendre functions. $\mathbf{P}(\mathbf{0})$ is (upper) triangular.

In addition, since the associated Legendre polynomials are defined as

$$P_{\ell m}(0) = \begin{cases} (-1)^p \dfrac{(2\ell+2m)!}{2^\ell p!(p+m)!} & \text{if } \ell - m = 2p, \quad (22a) \\ 0 & \text{if } \ell - m = 2p+1, \quad (22b) \end{cases}$$

all of the $\mathbf{P}(\mathbf{0})_{ii}$ diagonal elements are different from zero – thus this matrix is invertible.

The inverse of $\mathbf{P}(\mathbf{0})$ is also upper triangular and keeps the peculiar structure of the original matrix: in both $\mathbf{P}(\mathbf{0})$ and $\mathbf{P}(\mathbf{0})^{-1}$ only the $\ell - m = 2p$ terms differ from zero.

3.3 Comparison between the analytic and the numerical transformations

One way of comparing the two methods of calculating the Fourier spectrum is to look at what happens when a single $\mathcal{C}_\ell$ coefficient is different from zero. This is done in Fig. 6 for the case where $\mathcal{C}_{300} = 1$.

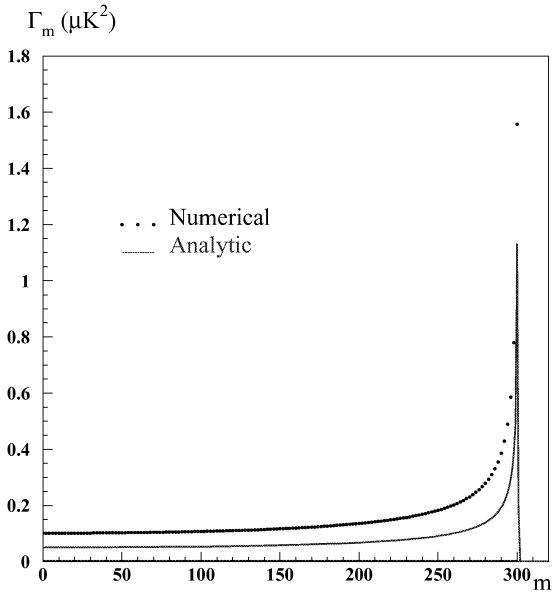

Figure 6. Middle curve (solid line): Fourier spectrum obtained using equation (17) when only $\mathcal{C}_{300} \neq 0$. We have used $\sigma = 0.5$ in equation (B2). Upper and lower set of points: the Γ_m coefficients computed with the $\mathbf{P}(\mathbf{0})$ matrix. Since we assume here that $\Theta = \pi/2$, all Γ_m coefficients for which the indices m are odd vanish.

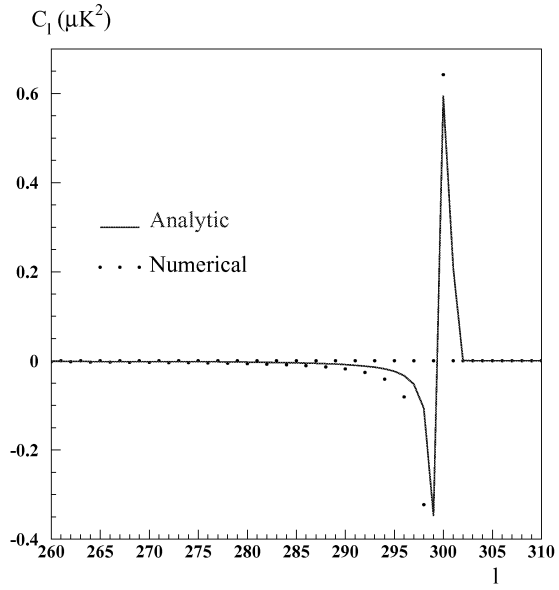

Figure 7. Solid line: the $\mathcal{C}_\ell$ spectrum obtained with equation (19) when only $\Gamma_{300} \neq 0$ (we have set $\sigma = 1$ in equation B2). Dots: the C_ℓ coefficients calculated using the $\mathbf{P}(\mathbf{0})^{-1}$ matrix.

Note that because we assume that $\Theta = \pi/2$ here, equation (22b) implies that all Γ_m coefficients with an odd index vanish (for a single non-vanishing C_ℓ coefficient with an odd ℓ value, all Γ_m coefficients with an even index would vanish). One notices that the $\Gamma(m)$ function runs at mid-height of the non-vanishing Γ_m coefficients.

Conversely, one may look at the $\mathcal{C}(\ell)$ function, which corresponds to the case where a single Γ_m Fourier coefficient is different from zero as shown in Fig. 7 (here we used $\Gamma_{300} \neq 0$). The fact that the $\mathcal{C}(\ell)$ graph is negative in some domain of ℓ values shows that no distribution of temperature inhomogeneities which satisfies the validity conditions of equation (4) (isotropy and Gaussian $a_{\ell m}$) can correspond to a Fourier spectrum with a single non-vanishing coefficient.

Taken together, Figs 6 and 7 show where we should expect a strong signal in one spectrum when the other spectrum presents a high power in some particular bins.

4 WORKING WITH SMALLER RINGS ON THE SKY ($\Theta < \pi/2$)

4.1 General features of the Fourier spectrum

In the preceding section we assumed that the scanned rings are the largest ones on the sphere ($\Theta = \pi/2$). In this case the fact that the $\mathbf{P}(\mathbf{0})$ matrix is invertible establishes that the Fourier spectrum of such rings contains all the physical information carried by the $\mathcal{C}_\ell$ coefficients.

Scanning smaller circles on the sky implies a higher fundamental frequency in Fourier angular space and thus a less dense sampling of this Fourier space.

In fact, the loss of information is then twofold.

(i) First, the $G(\mu) \equiv m\Gamma(m, \Theta)$ function is no longer measured for $\mu = 1$: the lowest value of μ that can be reached with the data is now $\mu = 1/\sin\Theta$.

(ii) Secondly, $G(\mu)$ is no longer measured for μ values that differ by one but for μ values that differ by $1/\sin\Theta$. As a very simple example: if the scan is performed for $\Theta = \pi/6$, then one measures $G(\mu)$ only for $\mu = 2n$ with $n \in [0, \ell_{\max}/2]$. Because of the smoothness of the angular spectra, this sparse sampling of the function $G(\mu)$ is not necessarily a drawback as long as the accuracy of the measurements compensates for it.

4.2 Analytic calculation of the $\mathcal{C}_\ell$ spectrum for $\ell > 1/\sin\Theta$

As far as the analytic calculation of the $\mathcal{C}_\ell$ spectrum is concerned, it can be performed with the same formalism as above (cf. Section 3.1). One should merely replace the derivative of $\Gamma(m, \pi/2)$ that appears in the right-hand side of equation (19) by the derivative (with respect to m) of

$$\tilde{\Gamma}(m) = \sin\Theta \sum_{i=1}^{\ell_{\max}\sin\Theta} \Gamma_i f(m\sin\Theta - i). \tag{23}$$

$\tilde{\Gamma}(m)$ is just the rescaled version (cf. equation 16) of $\Gamma(m, \Theta)$ defined by equation (B3) (this rescaling translates the $\Gamma(m, \Theta)$ Fourier spectrum into that corresponding to $\Theta = \pi/2$). Furthermore, the width of the interpolating function $f(x)$ of Appendix B (see equation B2) should be increased by a factor of $1/\sin\Theta$.

4.3 Numerical calculation of the $\mathcal{C}_\ell$ spectrum for $\ell > 1/\sin\Theta$

It follows from Section 4.1 above that the $\Gamma_m(\Theta)$ coefficients differ significantly from zero in the range $1 \leqslant m \leqslant \ell_{\max}\sin\Theta$. Then using the $\Gamma(m, \Theta)$ function that interpolates these coefficients and equation (16) one can calculate the following set of $\ell_{\max} - \ell_{\min} + 1$ values:

$$\tilde{\Gamma}_{m'} = \sin\Theta\Gamma(m'\sin\Theta, \Theta), \tag{24}$$

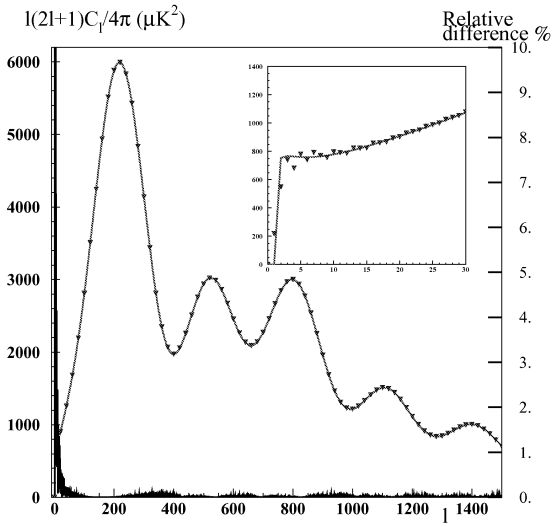

Figure 8. The input C_ℓ spectrum (solid curve) and the one reconstructed by the numerical method in the $\Theta = 40^\circ$ case (only some points are shown). The relative difference between the two spectra is shown by the lower curve (in per cent, right-hand scale). Inset: close-up of the low-ℓ region.

with $m' = \ell_{\rm min}, \ell_{\rm min}+1, \ldots, \ell_{\rm max}$, where $\ell_{\rm min}$ is the first integer larger than $1/\sin\Theta$. These $\tilde{\Gamma}_{m'}$ coefficients are those of the Fourier spectrum for $\Theta = \pi/2$. Once obtained, the C_ℓ spectrum is simply given by

$$\boldsymbol{\mathcal{C}} = \mathbf{P}(\mathbf{0})^{-1}\tilde{\boldsymbol{\Gamma}} \tag{25}$$

for $\ell \geqslant \ell_{\rm min}$. The $\mathbf{P}(\mathbf{0})$ matrix and its inverse have been discussed in Section 3.2. The first $\ell_{\rm min}-1$ rows and columns of $\mathbf{P}(\mathbf{0})^{-1}$ should be omitted in equation (25) since the lowest value of the m' index is $\ell_{\rm min}$.

Fig. 8 shows a numerical example: we use the 'typical' C_ℓ spectrum of Fig. 1 to produce a set of Γ_m values in the $\Theta = 40^\circ$ case (equation 4). Then we apply the method described above and compare the input spectrum with the obtained one. In this example we used a simple linear interpolation of the Γ_m spectrum. The agreement is excellent and better than that obtained with the analytic method (cf. Fig. 5) as the latter involves some approximations (cf. Section 2) in addition to those stemming from the scaling and the interpolation procedures.

The excellent agreement of Fig. 8 breaks down for low values of ℓ. Nevertheless, for $\ell \gtrsim 3$ in the $\Theta = 40^\circ$ case, one obtains an agreement of better than 10 per cent (far above the cosmic variance). For the case of $\Theta = 80^\circ$ our simple scaling method can be used up to an accuracy of better than 1 per cent for any ℓ values.

5 CONCLUSION

We have shown how data taken on circles with different colatitude angles Θ can be combined using a scaling law that is satisfied by the $m\Gamma_m(\Theta)$ coefficients at the 0.1 per cent level over a wide range of m and Θ values.

We have derived this scaling property from both geometrical considerations and linear expressions of the Γ_m coefficients in terms of the C_ℓ ones by introducing analytic approximations of the normalized Legendre associated polynomials $\mathcal{P}_{\ell m}(\cos\Theta)$ that enter these relations.

Integral equations were obtained that relate to a good approximation interpolating functions of the two sets of coefficients (Γ_m and C_ℓ). These analytic relations give a simple picture of the connection between the two types of spectra and are easy to use.

Finally, we have investigated ways of calculating the C_ℓ coefficients when the Γ_m Fourier spectrum is known. We have shown how the inverse of the $\mathcal{P}^2_{\ell m}(0)$ matrix can be used to perform this calculation not only for $\Theta = \pi/2$ but also in the general case where $\Theta < \pi/2$. This was achieved by, on the one hand, taking advantage of the scaling of the $m\Gamma_m$ spectrum and of its smoothness on the other hand.

This set of results provides a basis for further investigation of the connection between the measured C_ℓ and Γ_m spectra altered by noise and errors.

REFERENCES

Benoît A. et al., 2003, A&A, 399, L19
Bond J.R., Efstathiou G., 1987, MNRAS, 226, 655
Contaldi C.R. et al., 2002, in Proc. XVIII IAP Coll., On the Nature Of Dark Energy. Editions Frontiéres, Gif-sur-Yvette, in press (astro-ph/0210303)
Delabrouille J., Gorski K.M., Hivon E., 1998, MNRAS, 298, 445
Halverson N.W. et al., 2002, ApJ, 568, 38
Hanany et al., 2000, ApJ, 545, L5
Hu W., Dodelson S., 2002, ARA&A, 40, 171
Kraznov M. et al., 1977, Equations Intégrales. Editions Mir, Moscou
Mauskopf P.D. et al., 2000, ApJ, 536, L59
Piat M., Lagache G., Bernard J.P., Giard M., Puget J.L., 2002, A&A, 393, 359
Robin L., 1959, Fonctions Sphériques de Legendre et Fonctions Sphéroïdales, Vol. 3. Gauthier-Villars, Paris
Seljak U., Zaldarriaga M., 1996, A&A, 469, 437
Taylor A.C. et al., 2003, MNRAS, 341, 1066

APPENDIX A: APPROXIMATE EXPRESSIONS OF THE NORMALIZED LEGENDRE ASSOCIATED POLYNOMIALS

We start with asymptotic expressions of the Legendre functions obtained by Robin (1957) in the limit of large ℓ, with m/ℓ being kept constant. These asymptotic expressions depend on the relative value of m and $\ell\sin\Theta$.

(i) For $\ell < m/\sin\Theta$,

$$P_{\ell m}(\cos\Theta) \simeq \frac{(-1)^m \ell!}{\sqrt{2\pi}(\ell-m)!}\frac{(\ell\cos\Theta + M)^{\ell+\frac{1}{2}}(m\cos\Theta - M)^m}{\ell^{\ell+\frac{1}{2}}(\ell-m)^m M^{1/2}\sin^m\Theta}, \tag{A1}$$

where $M = \sqrt{m^2 - l^2\sin^2\Theta}$,

(ii) while for $\ell > m/\sin\Theta$,

$$P_{\ell m}(\cos\Theta) \simeq (-1)^m\sqrt{\frac{2}{\pi}} \times \frac{\ell!(\ell-m)^{\frac{\ell-m}{2}+\frac{1}{4}}(\ell+m)^{\frac{\ell+m}{2}+\frac{1}{4}}}{(\ell-m)!\ell^{\ell+\frac{1}{2}}N^{1/2}}\cos\omega, \tag{A2}$$

where

$$N = \sqrt{\ell^2\sin^2\Theta - m^2}, \tag{A3}$$

$$\omega = \left(\ell+\frac{1}{2}\right)\alpha - m\beta - \frac{\pi}{4}, \tag{A4}$$

$$\alpha = \arg(\ell\cos\Theta + \mathrm{i}N), \tag{A5}$$

$$\beta = \arg(m\cos\Theta + \mathrm{i}N). \tag{A6}$$

To 'normalize' these polynomials and obtain the $\mathcal{P}_{\ell m}$ values, they must be multiplied by

$$\sqrt{\frac{2\ell+1}{4\pi}\frac{(\ell-m)!}{(\ell+m)!}}. \tag{A7}$$

Then the last step consists in using Stirling's formula ($n! \simeq \sqrt{2\pi}n^{n+1/2}\mathrm{e}^{-n}$) to replace the factorials by analytic functions. A few simplifications can then be made that lead to the approximate expressions used in Section 2.

APPENDIX B: INTERPOLATING FUNCTIONS OF THE DISCRETE POWER SPECTRA

Since the calculation of the C_ℓ coefficients involves integrals over spherical Bessel j_ℓ functions (see e.g. Seljak & Zaldarriaga 1996), one may try and use an expression for these functions that extends them to non-integer values of j. However, here we will adopt a much simpler procedure and write

$$\mathcal{C}(\ell) \equiv \sum_{i=1}^{\ell_{\max}} \mathcal{C}_i\, f(\ell - i), \tag{B1}$$

where ℓ is now real, for which the value ranges between 2 (recall that we ignore the dipole term) and $\ell_{\max}$, and $f(x)$ is a positive, infinitely differentiable function ($f \in \mathcal{C}^\infty$), which differs significantly from 0 in an $|x|$ range which is of the order of unity, and the integral of which over x is unity. In practice we used

$$f(x) = \frac{1}{\sqrt{2\pi}\sigma}\exp\left(\frac{-x^2}{2\sigma^2}\right) \tag{B2}$$

with $\sigma \sim 1$.

Similarly, we define an interpolating function for the $\Gamma_m(\Theta)$ coefficients in the following way:

$$\Gamma(m, \Theta) \equiv \sum_{i=1}^{\ell_{\max}\sin\Theta} \Gamma_i\, f(m - i), \tag{B3}$$

where m is a real and $f(x)$ is chosen as above.

APPENDIX C: INVERSION OF THE INTEGRAL EQUATION RELATING $\mathcal{C}(\ell)$ TO $\Gamma(m)$

Since $\mathcal{C}(\ell)$ vanishes for $\ell > \ell_{\max}$, the integral equation (17) is of the form

$$\Gamma(m) = \int_0^\infty h(m\cosh x)\,\mathrm{d}x. \tag{C1}$$

We differentiate both sides of this equation with respect to m, substitute for this variable m the product $u\cosh\psi$, and integrate both sides over ψ between the limits 0 and ∞. We thus obtain

$$\int_0^\infty \Gamma'(u\cosh\psi)\,\mathrm{d}\psi = \int_0^\infty \mathrm{d}x \int_0^\infty h'(u\cosh\psi\cosh x)\cosh x\,\mathrm{d}\psi. \tag{C2}$$

Then a new integration variable ξ is used in the second integral of the right-hand side of this equation, defined by $\cosh\xi = \cosh\psi\cosh x$. Some simple algebra then leads to

$$\int_0^\infty \Gamma'(u\cosh\psi)\,\mathrm{d}\psi = \int_0^\infty \mathrm{d}x \int_x^\infty \frac{h'(u\cosh\xi)\sinh\xi\cosh x}{\sqrt{\sinh^2\xi - \sinh^2 x}}\,\mathrm{d}\xi. \tag{C3}$$

Once the integration order is reversed in the right-hand side of this equation one obtains

$$\int_0^\infty \Gamma'(u\cosh\psi)\,\mathrm{d}\psi = \int_0^\infty h'(u\cosh\xi)\sinh\xi\,\mathrm{d}\xi \int_0^\xi \frac{\cosh x\,\mathrm{d}x}{\sqrt{\sinh^2\xi - \sinh^2 x}}. \tag{C4}$$

The integral over x is simply $\pi/2$. Furthermore, $h(\infty) = 0$ in our case, so that

$$h(u) = -\frac{2u}{\pi}\int_0^\infty \Gamma'(\xi\cosh\psi)\,\mathrm{d}\psi. \tag{C5}$$

This paper has been typeset from a TEX/LATEX file prepared by the author.